Rock and Soil Mechanics

Volume 44 | Issue 7 Article 3

11-3-2023

Upper bound analysis of uplift piles in saturated clay and soil plug effect

Ke-wen ZHU
Key Laboratory of Geotechnical and Underground Engineering of Ministry of Education, Tongji University, Shanghai 200092, China; Department of Geotechnical Engineering, Tongji University, Shanghai 200092, China, zhukw19@tongji.edu.cn

Jian YU
Key Laboratory of Geotechnical and Underground Engineering of Ministry of Education, Tongji University, Shanghai 200092, China; Department of Geotechnical Engineering, Tongji University, Shanghai 200092, China, 002yujian@tongji.edu.cn

Mao-song HUANG
Key Laboratory of Geotechnical and Underground Engineering of Ministry of Education, Tongji University, Shanghai 200092, China; Department of Geotechnical Engineering, Tongji University, Shanghai 200092, China

Recommended Citation

ZHU, Ke-wen; YU, Jian; and HUANG, Mao-song (2023) "Upper bound analysis of uplift piles in saturated clay and soil plug effect," *Rock and Soil Mechanics*: Vol. 44: Iss. 7, Article 3.
DOI: 10.16285/j.rsm.2022.6185
Available at: https://rocksoilmech.researchcommons.org/journal/vol44/iss7/3

Upper bound analysis of uplift piles in saturated clay and soil plug effect

Abstract

A new mechanism is established and applied to the upper bound analysis of uplift piles in saturated clay. Upper bound solutions of uplift capacities of closed and open-ended piles are analyzed. The new mechanism is verified by comparing with elastoplastic finiteelement, existing lower bound and API solutions. Its reliability is assessed through case studies including one centrifuge test and two field tests. The effects of the pile length-diameter ratio, pile surface roughness, non uniformity of undrained soil strength and length of soil plug on the uplift bearing capacity are considered. A formulation predicting the net bearing capacity of closed-ended uplift piles in clay is proposed. The results show that an approximately linear relationship can be established between the normalized net bearing capacity coefficient and the pile length-diameter ratio for closed-ended piles. As for open-ended pipe piles, the ratio of the net bearing capacity coefficient of open ended pipe piles to that of closed-end piles tends to increase with the increase of the pile length-diameter ratio. The increase in the length of soil plug leads to an increase in the net bearing capacity coefficient of open-ended pipe piles. Therefore, the effect of soil plug should not be ignored.

Keywords

uplift pile, limit analysis method, nonhomogeneous clay, soil plug

Rock and Soil Mechanics 2023 44(7): 1995−2004 ISSN 1000−7598
https: //doi.org/10.16285/j.rsm.2022.6185 http://rocksoilmech.researchcommons.org/journal

Upper bound analysis of uplift piles in saturated clay and soil plug effect

ZHU Ke-wen[1, 2], YU Jian[1, 2], HUANG Mao-song[1, 2]

1. Key Laboratory of Geotechnical and Underground Engineering of Ministry of Education, Tongji University, Shanghai 200092, China
2. Department of Geotechnical Engineering, Tongji University, Shanghai 200092, China

Abstract: A new mechanism is established and applied to the upper bound analysis of uplift piles in saturated clay. Upper bound solutions of uplift capacities of closed and open-ended piles are analyzed. The new mechanism is verified by comparing with elastoplastic finite-element, existing lower bound and API solutions. Its reliability is assessed through case studies including one centrifuge test and two field tests. The effects of the pile length-diameter ratio, pile surface roughness, non-uniformity of undrained soil strength and length of soil plug on the uplift bearing capacity are considered. A formulation predicting the net bearing capacity of closed-ended uplift piles in clay is proposed. The results show that an approximately linear relationship can be established between the normalized net bearing capacity coefficient and the pile length-diameter ratio for closed-ended piles. As for open-ended pipe piles, the ratio of the net bearing capacity coefficient of open-ended pipe piles to that of closed-end piles tends to increase with the increase of the pile length-diameter ratio. The increase in the length of soil plug leads to an increase in the net bearing capacity coefficient of open-ended pipe piles. Therefore, the effect of soil plug should not be ignored.

Keywords: uplift pile; limit analysis method; nonhomogeneous clay; soil plug

1 Introduction

Uplift piles are widely used in geotechnical underground engineering. For example, anti-floating piles in large basements and some pile foundations of multi-pile jackets are subjected to large uplift loads. The calculation of uplift bearing capacity is of great significance to engineering safety. Therefore, it is necessary to investigate the calculation method of the bearing capacity of uplift piles. At present, the calculation methods of bearing capacity of vertically loaded piles proposed by the international mainstream API specification[1] and China's offshore oil and gas industry standard (SY/T 10030−2000)[2] are based on the limit equilibrium method. The pile side resistance and tip resistance are calculated separately and superimposed directly. Obviously, the pile shaft resistance and tip resistance do not necessarily reach their limits simultaneously, and these methods cannot consider the interaction between the pile shaft resistance and tip resistance. For the calculation of the bearing capacity of uplift piles, it is conservative to ignore the contribution of the pile bottom to the bearing capacity (especially for single piles of offshore wind turbine with large diameters). It may underestimate the bearing capacity of the pile foundation. In addition, in practical engineering, a large number of uplift piles are open-ended piles. They are different from the traditional closed-ended piles. The soil around the pile end will continue to pour into the pipe pile to form a soil-core during the sinking process of the open-ended pipe pile. When the height of the soil-core stops increasing, the soil-plug is formed. At present, the research mainly focuses on the working mechanism of pipe piles containing soil-cores in sandy foundations[3−9]. There are few studies on the soil-plug effect of open-ended piles in common clay in coastal areas. How to calculate the bearing capacity of pipe piles containing soil-plugs in such grounds is still a problem to be explored. The API specification does not explicitly address how to consider the effect of soil-plug on the bearing capacity of pipe piles. Therefore, the calculation method given by API is empirical with great limitations.

The upper bound limit analysis method has a rigorous theoretical basis. The upper bound of the bearing capacity of any hypothetical failure mechanism can be obtained by constructing an admissible velocity field. It is of greatly practical value for stability analysis of geotechnical engineering. The upper bound method has been widely used in the calculation of the bearing capacity of the shallow circular foundation. Kusakabe et al.[10] derived the upper bound solution of the bearing capacity of a circular footing with a smooth bottom and rough bottom on heterogeneous clay by using Hill and Prandtl failure modes, respectively. Hu et al.[11], Yun and, Bransby[12] and Wang et al.[13] carried out the upper bound analysis of the bearing capacity of the skirted foundation with the embedment ratio less than 5, and the results were compared with the finite element results. In recent years, Zhang et al.[14] used the Prandtl failure mode to solve the upper bound bearing capacity of the circular foundation on sand. Zhu et al.[15−16] derived the upper bound solution for the uplift bearing capacity of the suction caisson foundation based on the idea of the

Received: 1 August 2022 Accepted: 25 October 2022
This work was supported by the Natural Science Foundation of Shanghai (23ZR1468500) and the National Natural Science Foundation of China (51579177).
First author: ZHU Ke-wen, male, born in 1994, PhD candidate, focusing on geotechnical stability. E-mail: zhukw19@tongji.edu.cn
Corresponding author: YU Jian, male, born in 1987, PhD, Associate Professor, mainly engaged in teaching and research work in geotechnical engineering. E-mail: 002yujian@tongji.edu.cn

reverse bearing capacity. However, this method simplifies the energy calculation of the foundation sidewall to the overload of the soil on the same horizontal line at the bottom of the foundation, and the upper and lower bounds of the solution cannot be clearly judged. Therefore, the current upper bound analysis mainly focuses on shallow circular foundations, and there is still a lack of an admissible upper bound velocity field with a clear failure surface for pile foundations.

In view of the above problems, the upper-bound analysis mechanism and admissible velocity field of closed-ended and open-ended piles are first constructed in this paper. Then, the rationality of the proposed method is verified by comparison with the API calculation method, finite element solution and lower bound solution, as well as engineering case analysis. Subsequently, the parameter analysis is carried out, and the uplift bearing characteristics of the closed-ended pile are summarized. Then, the bearing capacity prediction formula of the closed-ended pile is fitted. Finally, the bearing capacity coefficient of the open-ended pile is linked to that of the closed-ended pile through their ratio relationship. The influences of the height of the soil plug, the inhomogeneity of soil strength and the friction coefficients of the inner and outer walls of the pipe pile on the uplift bearing capacity of the pipe pile are further discussed.

2 Problem description and upper bound admissible velocity field

2.1 Problem definition

In this paper, the uplift capacity of circular cross-section piles in saturated clay is analyzed. The problem is defined as shown in Fig. 1. Among them, L is the buried depth of the pile (pile length), and B is the diameter of the pile. Saturated clay can be approximately regarded as Trecsa material. Assuming that the unit weight of soil is γ, the undrained shear strength $s_{u(z)}$ changes linearly with the depth z:

$$s_{u(z)} = s_{u0} + \rho z \tag{1}$$

where s_{u0} is the undrained shear strength of clay at the ground surface; ρ is the slope of the undrained shear strength-depth curve. The nonuniformity of the soil strength is expressed by a normalized coefficient η:

$$\eta = \frac{s_{u0}}{s_{ub}} = \frac{s_{u0}}{s_{u0} + \rho L} \tag{2}$$

where s_{ub} is the undrained shear strength of clay at the depth of the pile bottom. When η is 1, it corresponds to homogeneous soil.

Similar to the definition of the ground bearing capacity coefficient, the normalized uplift bearing capacity coefficient N_c is defined as the ratio of the uplift bearing capacity per unit sectional area of the pile to the strength of soil at the bottom of the pile:

$$N_c = \frac{Q}{\pi b^2 s_{ub}} \tag{3}$$

where Q is the ultimate uplift bearing capacity; and b is the radius of the pile.

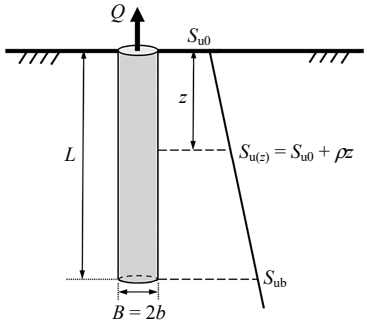

Fig. 1 Schematic graph of uplift piles in nonhomogeneous clay

2.2 Upper-bound mechanism of axisymmetric streamline velocity field

Huang et al.[17−18] derived the general solution of the streamline velocity field of limit analysis in undrained clay under the plane strain condition. The characteristics of the velocity field are as follows. The velocity field constructed based on the concept of streamline based velocity[19] is transmitted along a cluster of "streamlines" inside the deformation mechanism, and the deformation distribution of soil does not change in the direction perpendicular to the "streamline". The streamline cluster is obtained by geometric transformation (translation, scaling, etc.) through the characteristic streamline. The boundary shape is determined by characteristic streamline, and the external soil is rigid. Based on this, the streamline velocity field under the axisymmetric condition as shown in Fig. 2 can be derived, and the general solution is

$$\left.\begin{aligned} v_r &= \frac{1}{rc(z)} \cdot f\left[\frac{c(z)}{r-R}\right] \cdot \frac{\mathrm{d}c(z)}{\mathrm{d}z} \\ v_z &= \frac{1}{r(r-R)} \cdot f\left[\frac{c(z)}{r-R}\right] \\ v_\theta &= 0 \end{aligned}\right\} \tag{4}$$

where v_r, v_z and v_θ are the radial, vertical and circumferential velocities of soil, respectively; r is the cylindrical coordinate and $r = c(z)$ is an arbitrary characteristic streamline equation; $\mathrm{d}c(z)$ is the differential of $c(z)$; function $f(x)$ mainly controls the vertical component of the streamline velocity field; and R is the distance between the streamline domain and z-axis, which can be used to consider the width of the structure under the axisymmetric condition. It should be noted that for the non-uniform flow field, the streamline clusters will converge at the velocity singularity g', which should be excluded from the deformation zone to avoid singularity.

Figure 3 is the upper bound mechanism constructed in this paper. In the cylindrical coordinate system, the failure mechanism is composed of a triangular rigid block

https://rocksoilmech.researchcommons.org/journal/vol44/iss7/3
DOI: 10.16285/j.rsm.2022.6185

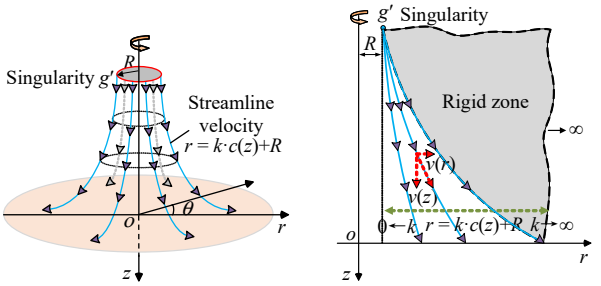

(a) 3D Sketch of axisymmetric streamlines (b) Sketch of axisymmetric streamlines in *r*-*z* plane

Fig. 2 Illustration of axisymmetric streamline velocity fields

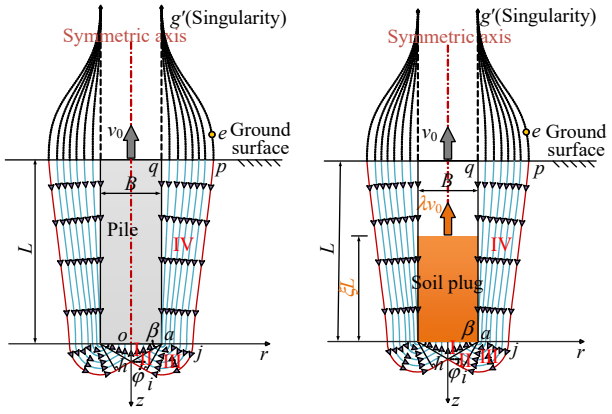

(a) Upper mechanism of closed-ended pile (b) Upper mechanism of open-ended pile

Fig. 3 Illustration of upper-bound mechanisms

aoh (Zone I) and three streamline velocity based plastic zones *ahi* (Zone II), *aij* (Zone III) and *ajpq* (Zone IV). As shown in Fig. 3(a), the failure mechanism below the pile bottom is similar to "Prandtl mechanism" in the ground bearing capacity problem. The geometry of the mechanism is determined by two angle optimization parameters β and φ. The soil (rigid block *aoh*) at the pile bottom of the mechanism moves upward at the same speed as the pile, and no detachment occurs. There are two reasons for this phenomenon: (1) Tang et al.[20] showed that there was a certain suction between the pile bottom and the soil under the pile bottom during the pullout of the uplift pile. Such suction will lead to the upward movement of soil at the pile bottom. (2) The soil considered in this paper is undrained clay. There is no volume change when the plastic deformation occurs. The soil on the pile side (Zone IV) in the mechanism flows downward. Due to the volume change being 0, the soil under the pile bottom will be squeezed upward. Therefore, the mechanism can ensure that the calculated result is the upper bound of the uplift capacity considering the suction effect from the perspective of the upper bound method. In order to ensure that the velocity directions of the streamline velocity based plastic zone III and the streamline velocity based plastic zone IV are consistent on the interface *a*-*j*, it can be assumed that the characteristic streamline equation of the streamline velocity field on the pile side (Zone IV) in *r*-*z* plane is

$$r = c(z) = \frac{s - z}{t^2 + z^2} + \frac{\arctan(z/t)}{t} \tag{5}$$

where s and t are the shape optimization parameters of the characteristic streamline. By controlling the coordinates of the maximum width point e on the streamline, the failure profile *p*-*j* on the pile side is optimized, in which parameter s is the vertical coordinate of point e, and parameter t is used to adjust the horizontal coordinates of point e. In the optimization process of solving the upper bound, controlling the position of point e (continuous optimization of parameters s and t) can provide a sufficient range of variation for the shape of Zone IV. It makes the optimization results of the upper bound calculation more accurate and reliable.

2.3 Construction of admissible velocity field of uplift pile

Let v_0 be the virtual velocity of the upward movement of the pile. Then, the radial and vertical velocities of Zone I can be derived from the velocity compatibility condition and the general solution of the "streamline" velocity field assumed in this paper:

$$\left.\begin{aligned} v_{r\mathrm{I}} &= 0 \\ v_{z\mathrm{I}} &= v_0 \end{aligned}\right\} \tag{6}$$

The radial and vertical velocities of Zone II are

$$\left.\begin{aligned} v_{r\mathrm{II}} &= \frac{v_0 \sin\varphi\cos\beta\left(b\tan\beta + r\tan\varphi - z\right)}{r\sin\left(\varphi+\beta\right)\tan\varphi\left(\tan\varphi+\tan\beta\right)} \\ v_{z\mathrm{II}} &= \frac{v_0 \sin\varphi\cos\beta\left(b\tan\beta + r\tan\varphi - z\right)}{r\sin\left(\varphi+\beta\right)\left(\tan\varphi+\tan\beta\right)} \end{aligned}\right\} \tag{7}$$

where β and φ are angle optimization parameters of the mechanism.

The radial and vertical velocities of Zone III are

$$\left.\begin{aligned} v_{r\mathrm{III}} &= \frac{v_0\cos\beta\left[\dfrac{b\sin\left(\varphi+\beta\right)}{\cos\beta} - \sqrt{\left(b-r\right)^2+z^2}\right]z}{r\left(\tan\varphi+\tan\beta\right)\sqrt{\left(b-r\right)^2+z^2}\cos\varphi\sin\left(\varphi+\beta\right)} \\ v_{z\mathrm{III}} &= \frac{v_0\cos\beta\left[\dfrac{b\sin\left(\varphi+\beta\right)}{\cos\beta} - \sqrt{\left(b-r\right)^2+z^2}\right]\left(b-r\right)}{r\left(\tan\varphi+\tan\beta\right)\sqrt{\left(b-r\right)^2+z^2}\cos\varphi\sin\left(\varphi+\beta\right)} \end{aligned}\right\} \tag{8}$$

On interface *a*-*j* between Zone III and Zone IV, since the condition of the consistent velocity direction is already satisfied in the construction of the characteristic streamline Eq. (5), it is only necessary to ensure that the vertical component of the velocity is equal on the interface. That is, the velocity compatibility can be ensured when $v_{z\mathrm{IV}}\big|_{z=0} = v_{z\mathrm{III}}\big|_{z=0}$. Therefore, the specific expression of function $f(x)$ in velocity field Eq. (4) in this paper is determined to be

$$f(x) = (x-1)b^2/x^2 \tag{9}$$

Therefore, the radial and vertical velocities of Zone

IV are

$$\left.\begin{aligned} v_{r\mathrm{IV}} &= b^2\frac{v_0}{r}\frac{\left[r-b-\dfrac{2bt^2\sec\beta\sin(\varphi+\beta)}{2s+\pi t}c(z)\right]\cdot}{\left[\dfrac{2bt^2\sec\beta\sin(\varphi+\beta)}{2s+\pi t}c(z)\right]^2}\\ &\quad\frac{r-b}{c(z)}\frac{\mathrm{d}c(z)}{\mathrm{d}z}\\ v_{z\mathrm{IV}} &= b^2\frac{v_0}{r}\frac{\left[r-b-\dfrac{2bt^2\sec\beta\sin(\varphi+\beta)}{2s+\pi t}c(z)\right]}{\left[\dfrac{2bt^2\sec\beta\sin(\varphi+\beta)}{2s+\pi t}c(z)\right]^2} \end{aligned}\right\} \quad (10)$$

According to the Eqs. (6)–(10), the velocity discontinuity only occurs on *a-h* and *a-q* interfaces. The velocity difference at *a-h* interface is

$$\Delta v_1 = \frac{\cos\varphi}{\sin(\varphi+\beta)}v_0 \quad (11)$$

The velocity difference on pile-soil interface *a-q* is

$$\Delta v_2 = \left[1-\frac{(2s+\pi t)}{2t^2\sec\beta\sin(\varphi+\beta)c(z)}\right]v_0 \quad (12)$$

3 External power and internal energy consumption rate

The upper bound theorem of limit analysis shows that in any hypothetical upper bound mechanism that satisfies the velocity compatibility condition, the internal energy consumption rate must be no less than the power done by the external force (external load and gravity). In the Tresca material, the upper bound theorem is expressed as[21]

$$\int_S T_i v_i \mathrm{d}S + \int_V f_i v_i \mathrm{d}V \leqslant \int_V 2s_\mathrm{u}\left|\dot{\varepsilon}_{\max}\right|\mathrm{d}V + \int_A s_\mathrm{u}\Delta v_\mathrm{t}\mathrm{d}A \quad (13)$$

where S is the boundary where the actual damage load T_i acts; V is the action zone of the body force f_i; $\dot{\varepsilon}_{\max}$ is the maximum principal strain rate; A is the area of the velocity discontinuity surface; and Δv_t is the velocity on the discontinuity surface.

In the theoretical derivation process of this paper, the internal energy consumption rate includes the energy consumption rate on the velocity discontinuity surface and the energy consumption rate in the streamline velocity based plastic zone. The external power is the virtual power done by the ultimate load and gravity.

3.1 Calculation of internal energy consumption rate

By examining the velocity fields of the streamline velocity based plastic zones II, III and IV, it can be seen that there is no friction energy consumption on the outer boundary *p-j-i-h* of the streamline velocity based plastic zones, and the work done by the internal force only occurs inside the zones. In the cylindrical coordinate system, the strain rate components in each direction are

$$\left.\begin{aligned} \dot{\varepsilon}_{ri} &= \frac{\partial v_{ri}}{\partial r}\\ \dot{\varepsilon}_{\theta i} &= \frac{v_{ri}}{r}\\ \dot{\varepsilon}_{zi} &= \frac{\partial v_{zi}}{\partial z}\\ \dot{\gamma}_{rzi} &= \frac{\partial v_{ri}}{\partial z}+\frac{\partial v_{zi}}{\partial r} \end{aligned}\right\} \quad (14)$$

where i = 2, 3, 4 correspond to Zones II, III, IV, respectively.

The maximum shear strain rate in the streamline velocity based plastic zone is

$$\left|\dot{\varepsilon}\right|_{\max i} = \frac{1}{2}\left(\dot{\varepsilon}_{\theta i}+\sqrt{\dot{\varepsilon}_{\theta i}^{\ 2}+4\dot{\gamma}_{zi}^{\ 2}-4\dot{\varepsilon}_{ri}\dot{\varepsilon}_{zi}}\right) \quad (15)$$

According to the geometric relationship of the mechanism in Fig. 3(a), the energy consumption rate E_2 of the streamline velocity based plastic Zone II is

$$E_2 = \int_0^{2\pi}\int_0^{b\cos\varphi\cos(\beta+\varphi)\sec\beta}\int_{(b-r)\tan\beta}^{r\tan\varphi+b\tan\beta}2\left|\dot{\varepsilon}\right|_{\max 2}r\mathrm{d}r\mathrm{d}\theta\mathrm{d}z + \int_0^{2\pi}\int_{b\cos\varphi\cos(\beta+\varphi)\sec\beta}^{b}\int_{(b-r)\tan\beta}^{(b-r)\cot\varphi}2\left|\dot{\varepsilon}\right|_{\max 2}r\mathrm{d}r\mathrm{d}\theta\mathrm{d}z \quad (16)$$

The energy consumption rate E_3 of the streamline velocity based plastic Zone III is

$$E_3 = \int_0^{2\pi}\int_{b\cos\varphi\cos(\beta+\varphi)\sec\beta}^{b}\int_{(b-r)\cot\varphi}^{\sqrt{(b\sec\beta\sin(\beta+\varphi))^2-(r-b)^2}}2\left|\dot{\varepsilon}\right|_{\max 3}r\mathrm{d}r\mathrm{d}\theta\mathrm{d}z + \int_0^{2\pi}\int_{b}^{b+b\sec\beta\sin(\beta+\varphi)}\int_{0}^{\sqrt{(b\sec\beta\sin(\beta+\varphi))^2-(r-b)^2}}2\left|\dot{\varepsilon}\right|_{\max 3}r\mathrm{d}r\mathrm{d}\theta\mathrm{d}z \quad (17)$$

The energy consumption rate E_4 of the streamline velocity based plastic Zone IV is

$$E_4 = \int_0^{2\pi}\int_b^{b+b\sec\beta\sin(\beta+\varphi)}\int_0^{c(z)}2\left|\dot{\varepsilon}\right|_{\max 4}r\mathrm{d}r\mathrm{d}\theta\mathrm{d}z \quad (18)$$

The friction energy consumption rate E_5 on velocity discontinuity interface *a-h* is

$$E_5 = \int_0^{2\pi}\int_0^{b}\int_0^{(b-r)\tan\beta}\Delta v_1 s_\mathrm{u}r\mathrm{d}r\mathrm{d}\theta\mathrm{d}z = \int_0^{2\pi}\int_0^{b}\int_0^{(b-r)\tan\beta}\Delta v_1 s_\mathrm{u}\frac{\cos\varphi}{\sin(\varphi+\beta)}v_0 r\mathrm{d}r\mathrm{d}\theta\mathrm{d}z \quad (19)$$

The friction energy consumption rate E_6 on pile-soil interface *a-q* is

$$E_6 = \int_0^{2\pi}\int_0^{b}\int_0^{L}\alpha_1 s_\mathrm{u}\Delta v_2 r\mathrm{d}r\mathrm{d}\theta\mathrm{d}z = \int_0^{2\pi}\int_0^{b}\int_0^{L}\alpha_1\cdot s_\mathrm{u}\left[1-\frac{(2s+\pi t)}{2t^2\sec\beta\sin(\varphi+\beta)c(z)}\right]v_0 r\mathrm{d}r\mathrm{d}\theta\mathrm{d}z \quad (20)$$

where α_1 is the roughness coefficient of the outer wall of the pile.

3.2 External power calculation

The external power to be calculated in this paper is

the power of gravity:

$$E_g = \overbrace{\gamma_p v_0 \pi b^2 L}^{\text{Power of pile weight}} + \overbrace{\sum_i \int_{V_i} \gamma_s v_z \mathrm{d}V_i}^{\text{Power of soil weight}} = \gamma_p v_0 \pi b^2 L + \gamma_s \sum_i \int_{V_i} v_z \mathrm{d}V_i \quad (21)$$

where γ_s and γ_p are the effective unit weight of soil and the average equivalent unit weight of pile, respectively.

According to the upper bound theorem, the problem of determining the ultimate bearing capacity of the uplift pile using the upper bound method can be transformed into the following mathematical optimization problem, in which the parameters to be optimized are the shape control parameters β and φ of the pile bottom failure mechanism and the shape optimization parameters s and t of the pile side failure mechanism.

$$N_c = \frac{Q}{\pi b^2 s_{ub}} = \frac{\min\left[\overbrace{E_2 + E_3 + E_4}^{\text{Plastic strain energy consumption rate}} + \overbrace{E_5 + E_6}^{\text{Firction energy consumption rate}} + \overbrace{E_g}^{\text{Gravity power}}\right]}{v_0 \pi b^2 s_{ub}} = N_{c0}^{c} + \overbrace{\left[\left(\gamma_p - \gamma_s\right) L / s_{ub}\right]}^{\text{Gravity item}} \quad (22)$$

where N_c is the bearing capacity coefficient; N_{c0}^{c} is the net bearing capacity coefficient of the closed-ended pile.

In Eqs. (6)−(22), the upper bound solution of the uplift bearing capacity of the closed-ended pile (see Fig. 3(a)) is derived. The upper bound calculation of the open-ended pipe pile (see Fig. 3(b)) is similar to that of the closed-ended pile. The difference is that there is a soil plug with a height of ξL ($0 \leqslant \xi \leqslant 1$, where ξ is the soil-plug height factor) in the pipe pile mechanism. Accordingly, the upper bound optimization parameter, i.e., virtual velocity λv_0 of soil plug motion ($0 \leqslant \lambda \leqslant 1$, where λ is the multiple) is introduced. At the same time, considering that the roughness of the inner and outer walls of the pipe pile may be different, it is necessary to distinguish the roughness coefficient α_1 of the outer wall of the pipe pile and the roughness coefficient α_2 of the inner wall of the pipe pile when calculating the upper bound of the open-ended pipe pile. Obviously, in the optimization process of the upper bound solution, when $\lambda = 0$, the soil plug does not move, and the soil around the pile does not flow. The mechanism failure occurs on interface *a-q* of the pile side wall in a "local" failure form. When $\lambda = 1$, the soil plug and the pile are pulled out at the same speed, and the mechanism failure occurs on *p-j-i-h* failure line in a "whole" failure form. The specific calculation process is not repeated here. It just needs to rewrite v_0 in Eqs. (6) to (10) as λv_0. It should be noted that the calculation of the friction energy consumption E_7 between the inner wall of the pipe pile and the soil plug is

$$E_7 = \int_0^{2\pi} \int_0^b \int_0^{\xi L} \alpha_2 s_u (1 - \lambda) v_0 r \mathrm{d}r \mathrm{d}\theta \mathrm{d}z \quad (23)$$

It should be noted that many scholars (such as Randolph et al.[3], Nicola et al.[22], etc.) pointed out that during the formation of soil plugs in pipe piles, the soil at a certain depth in the pipe wall will be compressed. It may lead to the increase of the soil density (unit weight) at this depth. However, this mechanism is too complicated to be quantitatively described in the current study. In order to simplify the calculation, this section does not consider the change in the weight of the soil plug in the pipe pile caused by the penetration of the pipe pile, and assumes that the average strength of the soil inside the pipe pile is the same as that outside the pipe pile. Therefore, the bearing capacity coefficient of the uplift pile considering the soil plug is

$$N_c = \frac{Q}{\pi b^2 s_{ub}} = \frac{\min\left[\overbrace{E_2 + E_3 + E_4}^{\text{Plastic strain energy consumption rate}} + \overbrace{E_5 + E_6 + E_7}^{\text{Firction energy consumption rate}} + \overbrace{E_g}^{\text{Gravity power}}\right]}{v_0 \pi b^2 s_{ub}} = N_{c0}^{o} + \overbrace{\left[G_p / (\pi b^2 s_{ub})\right]}^{\text{Gravity item}} \quad (24)$$

where G_p is the effective weight of the pipe pile (N); N_{c0}^{o} is the net bearing capacity coefficient of the open-ended pipe pile. From Eqs. (22) and (24), one can see that the gravity term does not affect the optimization results of the bearing capacity coefficient N_c. Therefore, only the net bearing capacity coefficients N_{c0}^{c} and N_{c0}^{o} are discussed in following sections.

4 Comparative verification

To verify the rationality of the upper bound mechanism in this paper, firstly, the calculation results are compared with the results of the API method and the finite element method, as well as the lower bound results in the existing literature. Then, the calculation results of this paper are compared with the measured data by combining some experimental data. It is noted that the roughness coefficient of the pile wall in the case analysis is taken according to the method recommended by literature [23].

4.1 Comparison with API method, finite element method and lower bound solution

In this paper, the elastoplastic finite element analysis is carried out by using the axisymmetric module of Plaxis software, and the results of the lower bound method in literature [24] are sorted out. The results of the upper bound analysis in this paper are compared with the results of the API method, elastoplastic finite element method and lower bound method. The finite element calculation is performed using the Plaxis software (version CE v20), which is widely used in the field of geotechnical engineering. The typical mesh division of the model is shown in Fig. 4. To eliminate the influence of the model boundary, the horizontal width of the model is 10*b* and the vertical height is 3*L*. The model adopts the 15-node axisymmetric mesh. The model is divided into 1 315 elements and 4 956 nodes. The linear elastic constitutive model is adopted for modelling pile with the elastic modulus of 1×10^9 kN /m^2 and Poisson's ratio of 0.3. The pile can be approximated as a rigid body

in the calculation. The Tresca constitutive model with elastic-perfectly-plastic is used for soil. The undrained strength of soil is s_u = 20 kPa; and the elastic modulus is $E = 200s_u$; and the Poisson's ratio is set as 0.499 to simulate the undrained condition. In this model, the pile-soil contact surface is set as the interface characteristics provided by the Plaxis software, which is consistent with the definition of the pile side roughness coefficient. Fig. 5 shows the comparison of the calculation results of the bearing capacity of closed-ended uplift piles in homogeneous clay. It can be seen that the results of this paper have the same trend with the results of the API method, finite element method and lower bound method. The average error of the results of this paper is about 10% compared with the finite element results, and the average error compared with the lower bound method is about 15%. It verifies the rationality of the present calculation method. The figure also displays that under the same roughness coefficient of the outer wall, the uplift bearing capacity calculated by the API method is lower than the results of the upper bound method, the elastic-plastic finite element method and the lower bound method. It is worth noting that the calculation results of the API method are about 7% lower than the results of the lower bound method on average. It confirms the conservative trend of the API calculation method. Fig. 6 shows the velocity field nephogram of closed-ended uplift piles with different length−diameter ratios (L/B = 5, 10 and 15) in homogeneous clay. The failure mechanism presents a form of "outward expansion". The horizontal failure area increases obviously as the length−diameter ratio increases, which is similar to that reported in literature [22].

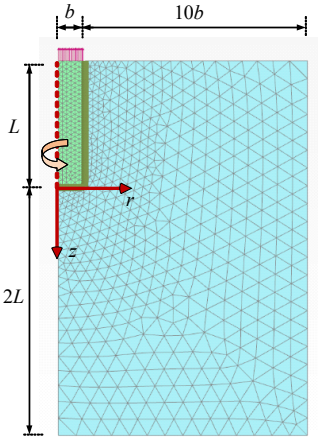

Fig. 4 Typical finite element mesh

4.2 Comparison with centrifugal tests

Jirasak[25] carried out centrifugal model tests on uplift piles at National University of Singapore. The test was performed under a gravity of 100g, and the Malaysian kaolin with a saturated unit weight of 16 kN /m^3 was used. The distribution of soil strength along the depth after consolidation measured by T-bar penetrometers was s_{uz} = 19+z (z is the depth (m)). The test pile was an aluminum closed-ended pile with a diameter of 1.2 cm, corresponding

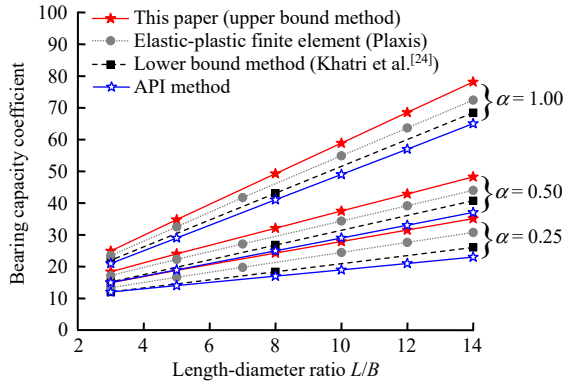

Fig. 5 Comparison of N_{c0} among the present upper-bound solution, API method, lower-bound method and FEM solution

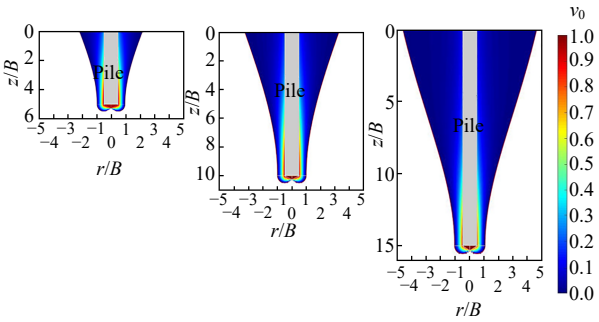

(a) L/B = 5 (b) L/B = 10 (c) L/B = 15

Fig. 6 Failure mechanisms of uplift piles in homogeneous clay

to the prototype diameter of 1.2 m. The test measured the bearing capacity of uplift piles with different length−diameter ratios. The measured bearing capacity was normalized and compared with that of this paper, as shown in Table 1. It shows that the calculation results of this paper are in good agreement with the measured results of centrifugal tests. The calculation results of this paper are slightly larger than the measured values. The average error is 10.4% and the minimum error is 4.0%. It proves that the method proposed in this paper has good reliability.

Table 1 Comparison of N_c among the present upper-bound solutions and centrifuge test results[25]

Test No.	Pile diameter /m	Length-diameter ratio L/B	Soil strength /kPa	Actual load /MN	Measurement N_c	This paper N_c
T1B	1.2	13.3	19+z	1.30	33.0	37.0
T1C	1.2	14.0	19+z	1.19	32.0	35.0
T1D	1.2	5.5	19+z	0.73	25.0	26.0
T2D	1.2	8.0	19+z	0.84	26.0	32.0
T3D	1.2	14.2	19+z	1.50	36.9	41.3
T1E	1.2	13.2	19+z	1.28	32.5	41.2
T2E	1.2	12.3	19+z	1.21	31.6	39.7
T3E	1.2	11.7	19+z	1.20	32.0	36.0
T1F	1.2	13.3	19+z	1.25	31.6	33.6
T2F	1.2	12.9	19+z	1.34	34.3	40.5
T3F	1.2	12.3	19+z	1.27	33.3	34.5

4.3 Comparison with actual project (Case 1)

Case 1 is the uplift tests of offshore platform cast-in-place piles carried out by Clarke et al.[26] in the "West Sole field" site in the North Sea, Europe. According to the geological survey report, the site soil is dominated

by silty clay. The average unit weight of soil is 18 kN /m^3, and the diameter of test piles is 0.76 m. The length−diameter ratio of test piles and the distribution of soil strength in different sites are summarized in Table 2. From the comparison between the measured bearing capacity and the calculated bearing capacity of the present method in Table 2, it can be seen that the maximum error between the two is 11.3%, and the minimum error is 2.7%. The error range is relatively small, which verifies the rationality of the calculation method proposed in this paper.

Table 2 Comparison of N_c among the present upper-bound solutions and filed test results of Case 1

Test No.	Pile diameter /m	Length−diameter ratio L/B	Soil strength /kPa	Actual load /kN	Measurement N_c	This paper N_c
A6T	0.76	7.9	200+6z	2 371	22.2	23.7
A12T	0.76	15.8	200+6z	4 349	37.8	38.0
A15T	0.76	19.7	200+6z	5 100	38.8	43.2
A18T	0.76	23.7	200+6z	6 568	47.0	48.9

4.4 Comparison with actual project (Case 2)

Case 2 is the in-situ uplift tests conducted by Almeida et al.[27] at four clay test sites. The geometric dimensions of the test piles and the strength distribution of soil in each site are shown in Table 3. It shows that the average error between the results of this paper and the measured results is 12.6%, and the minimum error is 6.4%. The present calculation method overestimates the actual bearing capacity but the error is still in a small range.

Table 3 Comparison of N_c among the present upper-bound solutions and filed test results of Case 2

Test No.	Pile diameter /m	Length−diameter ratio L/B	Soil strength /kPa	Actual load /kN	Measurement N_c	This paper N_c
LISDB2	0.812	12.3	8.5+0.7z	377	47.1	50.0
HAGA-B6	0.153	32.7	40.0	60	83.3	85.1
HAGA-A15	0.153	32.7	40.0	54	75.4	85.1
HAGA-A16	0.153	32.7	40.0	56	77.7	85.1
CWDNC	0.305	29.5	64.0+4.0z	400	54.8	59.6
CWDNE	0.305	29.5	64.0+4.0z	380	52.1	59.6

5 Parametric study and result analysis

To explore the influence of the length−diameter ratio, soil strength, soil−plug height, and roughness of inner and outer walls of the pipe pile on the upper bound uplift bearing capacity, detailed parametric analysis is carried out in this section.

5.1 Calculation results of upper bound net bearing capacity for closed-ended piles

Figure 7 shows the relationship between the normalized net bearing capacity coefficient of the closed-ended pile and the length−diameter ratio, the roughness coefficient of the outer wall and the non-uniformity coefficient of soil strength. One can see that there exists an approximate linear relationship between the normalized net uplift bearing capacity coefficient of the closed-ended pile and the length−diameter ratio (L/B) of the pile. The normalized net uplift bearing capacity coefficient increases with an increase in the roughness coefficient of the outer wall of the closed-ended pile and the non-uniformity coefficient of soil strength on the pile side. However, the roughness coefficient of the pile wall has a greater influence on the net bearing capacity than the non-uniformity coefficient of soil strength. To provide a convenient prediction formula for the bearing capacity of the closed-ended pile, nonlinear regression analysis is carried out based on the calculation results of parametric analysis in Fig. 7. The final prediction formula for the net bearing capacity coefficient is expressed as follows:

$$N_{c0}^{c}\left(\frac{L}{B},\alpha_1,\eta\right)=\left[(2\alpha_1+0.25)\eta+2\alpha_1+0.5\right]\frac{L}{B}+(0.25\alpha_1+1.2)\eta+(\alpha_1+8.25) \tag{25}$$

The final goodness of fit (the ratio of the sum of squares in regression analysis to the total sum of squares) is R^2 = 0.991. It suggests that the objective function can well reflect the upper bound calculation results.

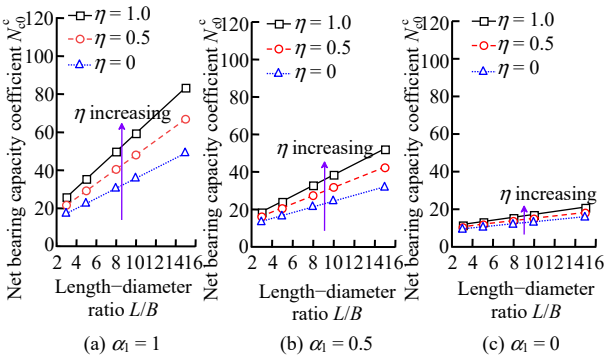

Fig. 7 Variation of N_{c0}^{c} with L/B for closed-ended piles

5.2 Calculation results of upper bound net bearing capacity for open-ended piles

Figures 8, 9 and 10 show the variation of the ratio (N_{c0}^{o}/N_{c0}^{c}) of the net uplift bearing capacity coefficient of the open-ended pipe pile to that of the closed-ended pile with the length−diameter ratio L/B when the non-uniformity coefficient η of soil strength on the pile side is 1.0, 0.5 and 0, respectively. It can be seen from Fig. 8 that when the soil plug is full of the pipe pile and the inner wall is completely rough (i.e., $\xi=1\cap\alpha_2=1$), the net uplift bearing capacity coefficient of the open-ended pipe pile is the same as that of the closed-ended pile (N_{c0}^{o}/N_{c0}^{c} = 1). It indicates that in this case the bearing behavior of the open-ended pipe pile is the same as that of the closed-ended pile. It should be noted that the net uplift bearing capacity coefficient of the pipe pile is always 0 when the inner and outer walls of the open-ended pipe pile are completely smooth.

Apart from the above two extreme cases, one can see from Figs. 8, 9 and 10 that the ratio of the net uplift bearing capacity coefficient of the open-ended pipe pile to that of the closed-ended pile increases with the increase of

the length−diameter ratio L/B. When the roughness coefficient α_1 of the outer wall of the pipe pile and the roughness coefficient α_2 of the inner wall are fixed, the net uplift bearing capacity of the pipe pile increases with the increase of the height coefficient ξ of the soil plug. It proves that the soil plug has a non-negligible influence on the uplift bearing capacity of the pipe pile.

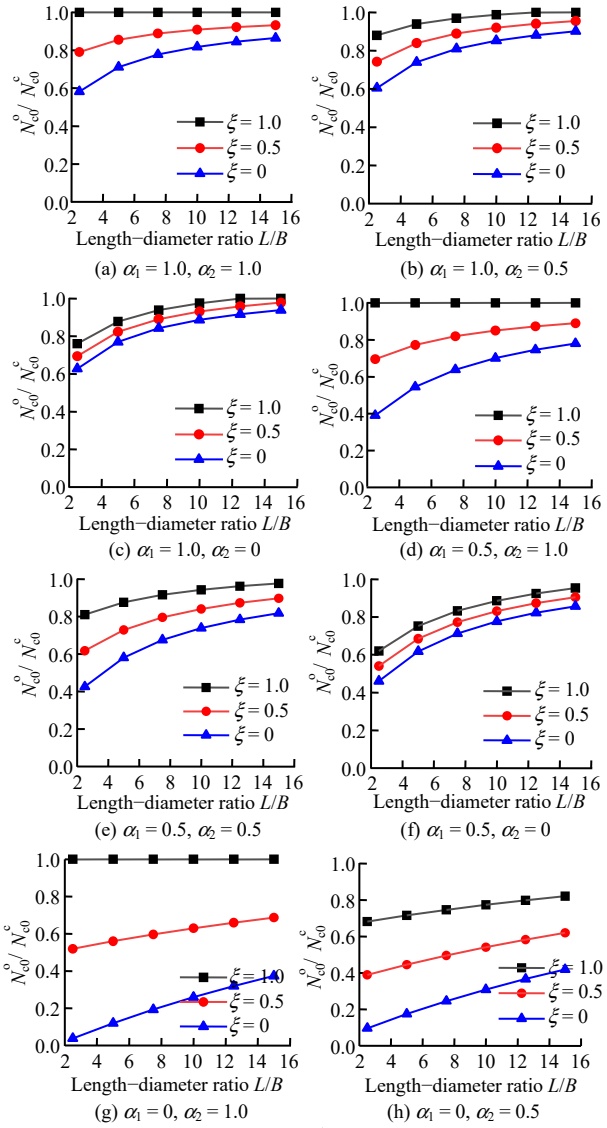

Fig. 8 Variation of N^o_{c0}/N^c_{c0} with L/B ($\eta = 1$)

Figures 8, 9 and 10 show the relationship between the net uplift bearing capacity coefficient of pipe pile and the pile length−diameter ratio, and the height of soil plug. Further studies are carried out on the influencing factors such as the soil non-uniformity coefficient and roughness of the pile inner and outer walls combining Figs. 8, 9 and 10 as well as Eq. (25). As shown in Fig. 11, when the inner and outer walls of the pile are completely rough and the soil plug height is 0.5 times the pile length ($\xi = 0.5$), the net uplift bearing capacity coefficient of the pipe pile increases with the increase of the soil non-uniformity coefficient. Fig. 11 illustrates the relationship between the net uplift bearing capacity coefficient of the pipe pile and the roughness coefficient of the outer wall when the

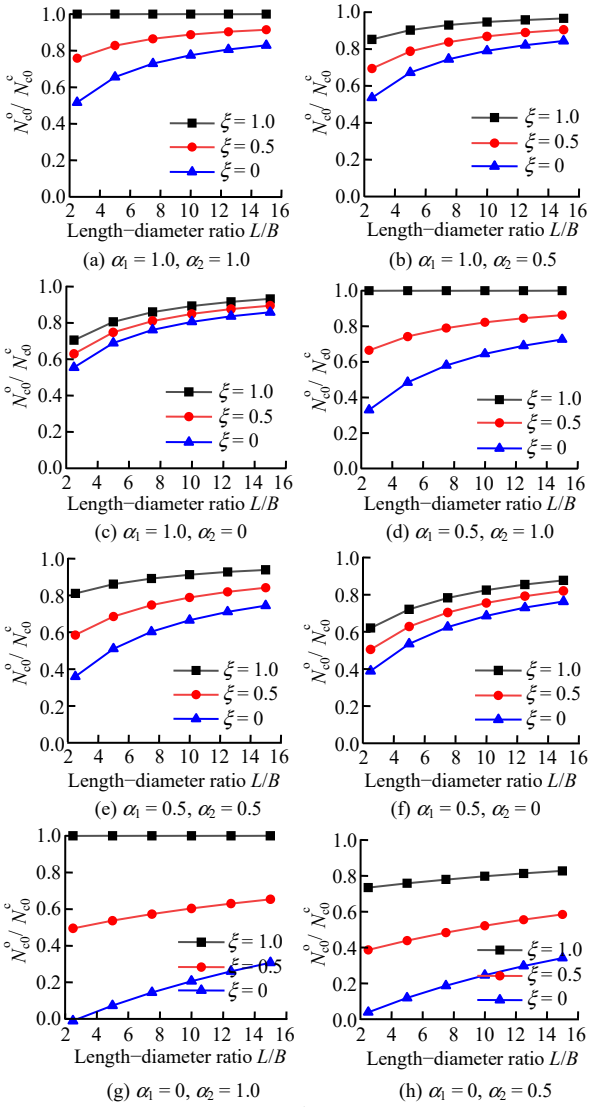

Fig. 9 Variation of N^o_{c0}/N^c_{c0} with L/B ($\eta = 0.5$)

inner wall of the pipe pile is completely rough and the height of the soil plug is 0.5 times the pile length ($\xi = 0.5$). Fig. 12 shows that the net uplift bearing capacity increases with the increase of the roughness coefficient of the outer wall. However, when the length−diameter ratio is small, the increase is not obvious. When the length−diameter ratio is large, the roughness coefficient of the outer wall of the pipe pile has a more significant effect on the net uplift bearing capacity coefficient.

Figure 13 shows the relationship between the net uplift bearing capacity coefficient and the roughness coefficient of the inner wall when the outer wall of the pipe pile is completely rough and the pipe pile is filled with the soil plug ($\alpha_1 = 1 \cap \xi = 1$). It can be seen from the calculation results that the roughness coefficient α_2 of the inner wall of the pipe pile affects the net uplift bearing capacity coefficient, and the influence is more significant for pipe piles with small length−diameter ratios. For pipe piles with different length−diameter ratios, when the roughness coefficient α_2 of the inner wall of the pipe pile is small, the net bearing capacity coefficient N^o_{c0} increases linearly with α_2, and finally no longer increases after reaching

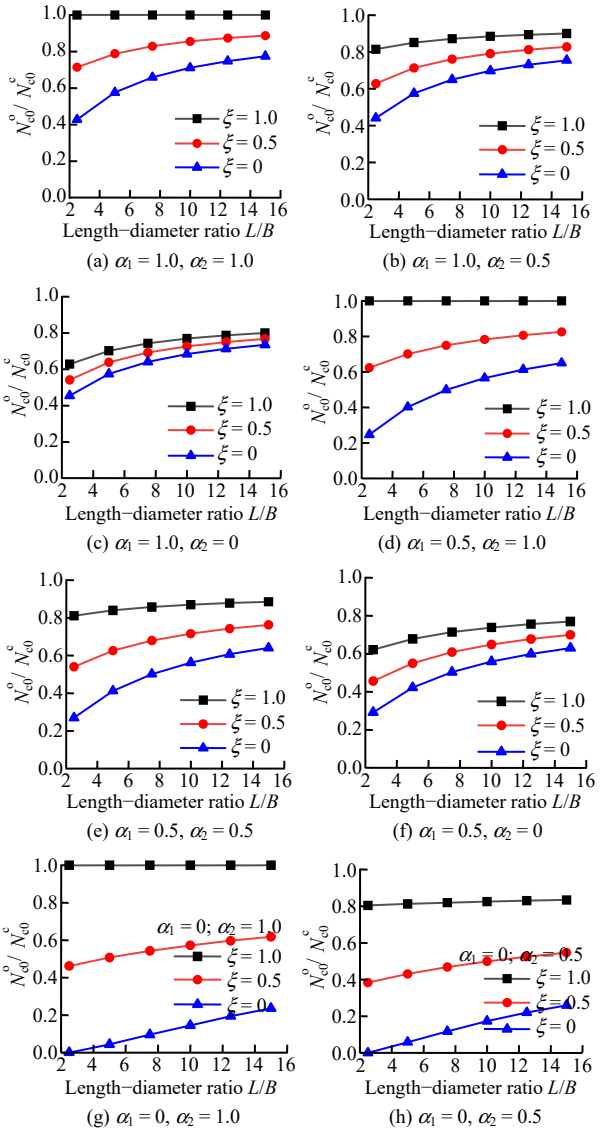

Fig. 10 Variation of N_{c0}^{o}/N_{c0}^{c} with L/B ($\eta = 0$)

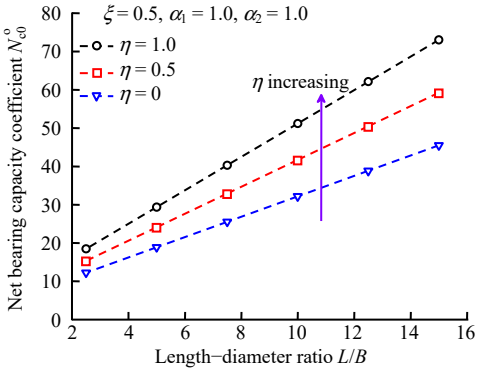

Fig. 11 Variation of N_{c0}^{o} with η for open-ended pipe piles

the maximum bearing capacity. This is mainly attributed to the fact that when the roughness coefficient of the inner wall of the pipe pile is small, the mechanism failure occurs on the pile wall, and the bearing capacity increases with the increase of the roughness coefficient of the inner wall. When the roughness coefficient reaches the critical value, the mechanism failure exhibits an overall failure. In this case, the failure mode of the open-ended pipe pile is the same as that of the closed-ended pile.

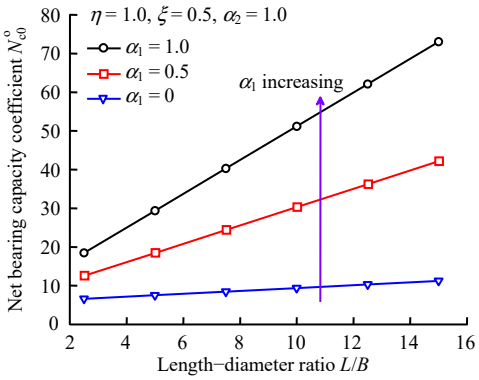

Fig. 12 Variation of N_{c0}^{o} with α_1 for open-ended pipe piles

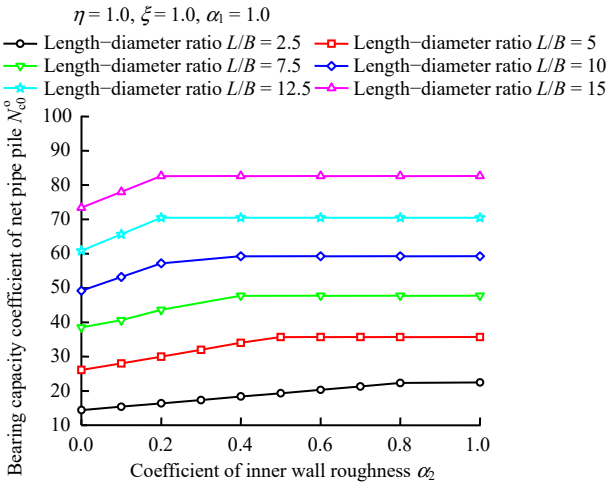

Fig. 13 Variation of N_{c0}^{o} with α_2 for open-ended pipe piles

6 Conclusions

In this paper, the upper bound analysis mechanism and the kinematically admissible velocity field of the uplift pile in saturated clay are constructed. Then, the upper bound solution of the uplift bearing capacity is derived. Finally, the proposed method is extended to the calculation of the uplift bearing capacity of the pipe pile considering soil plug. Specific conclusions are drawn as follows:

(1) This paper makes up for the conservative deficiency of the existing API calculation method. Through the example analysis and engineering case comparison, it shows that the calculation results of this paper are in good agreement with the test results, which verifies the feasibility and rationality of the theoretical analysis. Through parameter analysis, this paper gives the prediction formula of the upper bound uplift bearing capacity of the closed-ended pile and the ratio of the net bearing capacity of the open-ended pipe pile to that of the closed-ended pile. The results can provide significant references for future research.

(2) For the closed-ended pile, the normalized net uplift bearing capacity coefficient is approximately linear with the length−diameter ratio of the single pile, and increases with the increase of the roughness coefficient of the outer wall and the non-uniformity coefficient of soil strength on the pile side. However, the roughness coefficient of the pile side has a greater influence on the net bearing

capacity coefficient than the non-uniformity coefficient of soil strength.

(3) For the open-ended pipe pile, the net uplift bearing capacity of the pipe pile increases with the increase of the height of the soil plug. The soil plug has a non-negligible influence on the uplift bearing capacity of the pipe pile. The ratio of the net uplift bearing capacity coefficient of the open-ended pipe pile to that of the closed-ended pile increases with the increase of the length−diameter ratio L/B. When the soil is full of the pipe pile and the inner wall is completely rough, the net uplift bearing capacity coefficient of the open-ended pipe pile is the same as that of the closed-ended pile. The possible mechanism is that when the roughness coefficient of the inner wall of the pipe pile is small, soil failure occurs on the wall of the pipe pile, and the bearing capacity will increase with the increase of the roughness coefficient of the inner wall. When the roughness coefficient reaches a certain value, the mechanism failure exhibits an overall failure. In this case, the failure mode of the open-ended pipe pile is the same as that of the closed-ended pile.

References

[1] American Petroleum Institute. Recommended practice for planning, designing and constructing fixed offshore platforms[S]. [S. l.]: [s. n.], 2010.

[2] National technical committee of China for offshore Oil Engineering Standardization. SY/T 10030−2004 Recommended practice for planning, designing and constructing offshore platforms-working stress design[S]. Beijing: Petroleum Industry Press, 2004.

[3] RANDOLPH M F, LEONG, E C, HOULSBY G T. One-dimensional analysis of soil plugs in pipe piles[J]. Géotechnique, 1991, 41(4): 587−598.

[4] KOU H, CHU J, GUO W, et al. Pile load test of jacked open-ended prestressed high-strength concrete pipe pile in clay[J]. Proceedings of the Institution of Civil Engineers, 2018, 171(GE3): 243−251.

[5] ZHU Xiang-rong, YE Jun-neng, JIANG Xian-fang, et al. Preliminary analysis on load-bearing characteristics of driven-tube cast-in-place[J]. Chinese Journal of Geotechnical Engineering, 2003, 25(5): 538−542.

[6] LI Jian-qiang, ZHOU Jian. Effects on soil plugging and plugged mode in open-ended pile[J]. Rock and Soil Mechanics, 2008, 29(2): 449−454.

[7] ZHOU Jian, WANG Guan-ying. Development and expectation on soil plug in driving or jacked open-ended pipe piles[J]. Building Structure, 2008, 38(4): 25−29.

[8] ZHANG Zhong-miao, LIU Jun-wei, YU Feng, et al. Research on plugging effect of jacked prestressed concrete pipe pile[J]. Rock and Soil Mechanics, 2011, 32(8): 2274−2280.

[9] ZHAN Yong-xiang, YAO Hai-lin, DONG Qi-peng, et al. Study of process of open-ended pipe pile driven into sand soil by particle flow simulation[J]. Rock and Soil Mechanics, 2013, 34(1): 283−289.

[10] KUSAKABE O, SUZUKI H, NAKASE A. An upper bound calculation on bearing capacity of a circular footing on a non-homogeneous clay[J]. Soils and Foundations, 1986, 26(3): 143−148.

[11] HU Y, RANDOLPH M F, WATSON P G. Bearing response of skirted foundation on nonhomogeneous soil[J]. Journal of Geotechnical & Geoenvironmental Engineering, 1999, 125(11): 924−935.

[12] YUN G, BRANSBY M F. The undrained vertical bearing capacity of skirted foundations[J]. Soils and Foundations, 2007, 47(3): 493−505.

[13] WANG Jia-yu, LIU Run, JI Yong-hong, et al. Upper bound limit analysis of horizontal and moment ultimate bearing capacities of bucket foundation[J]. Rock and Soil Mechanics, 2022, 43(3): 777−788.

[14] ZHANG Guo-xiang, FU Jiang-shan. Upper bound solution for bearing capacity of circular shallow foundation based on limit analysis[J]. Rock and Soil Mechanics, 2010, 31(12): 3849−3854.

[15] ZHU Wen-bo, DAI Guo-liang, GONG Wei-ming, et al. Upper bound solution for ultimate bearing capacity of suction caisson foundation based on Prandtl failure mode[J]. Journal of Central South University (Science and Technology), 2019, 50(1): 158−164.

[16] ZHU Wen-bo, DAI Guo-liang, GONG Wei-ming, et al. Upper bound solution for ultimate bearing capacity of suction caisson foundation based on Meyerhof failure mode[J]. Journal of Southeast University (Natural Science Edition), 2018, 48(5): 828−833.

[17] HUANG M S, WANG H Y, YU J, et al. Undrained stability analysis of a plane strain circular tunnel using streamline velocity fields[J]. International Journal of Geomechanics, 2019, 19(5): 06019006.

[18] HUANG M S, WANG H Y, TANG Z, et al. Basal stability analysis of braced excavations in anisotropic and non-homogeneous undrained clay using streamline velocity fields[J]. Acta Geotechnica, 2020, 16(4): 1175−1186.

[19] TANG Zhen, HUANG Mao-song, YUAN Ju-yun. Upper bound analysis of basal stability of excavations based on continuous velocity fields[J]. Rock and Soil Mechanics, 2017, 38(3): 833−839.

[20] TANG C, PHOON K K, CHEN Y J. Statistical analyses of model factors in reliability-based limit-state design of drilled shafts under axial loading[J]. Journal of Geotechnical and Geoenvironmental Engineering, 2019, 145(9): 04019042.

[21] SHIELD R T, DRUCKER D C. The application of limit analysis to punch indentation problems[J]. Journal of Applied Mechanics, 1953, 20: 453−460.

[22] NICOLA A D, RANDOLPH M F. The plugging behaviour of driven and jacked piles in sand[J]. Géotechnique, 1997, 47(4): 841-856.

[23] KOLK H J, VELDE E D. A reliable method to determine friction capacity of piles driven into clays[C]// Proceedings of the 28th Offshore Technology Conference. Houston: [s. n.], 1996.

[24] KHATRI V N, KUMAR J. Uplift capacity of axially loaded piles in clays[J]. International Journal of Geomechanics, 2011, 11(1): 23−28.

[25] JIRASAK A. Centrifuge modeling of single pile subjected to compression and tension in clay[D]. Singapore: National University of Singapore.

[26] CLARKE J, LONG M M, HAMILTON J. The axial tension test of an instrumented pile in overconsolidated clay at Tilbrook Grange[C]//Large-scale Pile Tests in Clay. [S. l.]: Thomas Telford Publishing, 1993.

[27] ALMEIDA M S S, FERNANDO A B D, TOM L. Use of the piezocone test to predict the axial capacity of driven and jacked piles in clay[J]. Canadian Geotechnical Journal, 1996, 33(1): 23−41.